Magnetorheological Elastomers

Subjects: Polymer Science

Contributor: Muhammad Usman , Asad Hanif

Magnetorheological elastomers (MREs) are magneto-sensitive smart materials, widely used in various applications, i.e., construction, automotive, electrics, electronics, medical, minimally invasive surgery, and robotics. Such a wide field of applications is due to their superior properties, including morphological, dynamic mechanical, magnetorheological, thermal, friction and wear, and complex torsional properties.

magneto-sensitive smart materials,MREs

1. Introduction

The materials, i.e., piezoelectric [1][2], biomimetic [3], thermochromic [4], electrorheological [5], thermoelectric [6], photochromic [7], magneto-sensitive [8], magneto-active [9][10], and shape memory alloys [11], intelligently respond to variations in the surrounding conditions and are termed as smart materials [12]. The magnetorheological (MR) materials, invented by Jacob Rabinow in 1948, are magneto-sensitive smart materials [13][14]. These materials are produced in different forms, such as MR foams, MR elastomer (MRE), MR gel [15], and MR fluid (MRF) [16][17][18]. Although the response time of MRE is slower than MRF [19], MRE still effectively overcomes the deficiencies of MRF, particularly the particle sedimentation, leakage, and environmental contamination problems [20]. Due to their rapidly and reversibly controllable properties, including morphological [21], tomographical [22], mechanical [23], dynamic mechanical [24][25][26], magneto-mechanical [27][28], magneto-shear [29], rheological and melt rheological [30], complex torsional [31], physicochemical [32], thermal [33], friction and wear [34], fatigue life [35], and viscoelastic [12] properties, as well as a fail-safe feature [19], MREs have a wide range of applications. These applications include damping and smart sensing in vibration absorbers [19] and vibration isolators [36][37][38][39], other sensing devices [40][41], engine mounts, vehicle seat suspension [42], adaptive stiffness devices, actuators to control the flow [31], MR elastic polishing composites [43], seismic dampers and base isolators [44][45][46][47][48], multilayer MRE-based vibration isolators [49], MREs embedded beams [50], variable impedance surfaces, artificial muscles [24], deformable wings [51], MRE embedded sandwich plates [52], adaptive blades [53], active vibration isolation platforms [54][55][56], tunable absorption systems [57], MREs and MRFs based isolators [58], and dielectrics for plane capacitors [59][60]. MREs have also been used in soft, small-scale continuum robots with navigation and active steering capabilities [61]. The polydimethylsiloxane (PDMS)-based sterilizable and biocompatible MREs have recently been introduced for medical and cellular intervention. Moreover, MREs are the most suited candidates for minimally invasive surgery (MIS) and robotic MIS (RMIS) applications [62]. Several numerical studies and models investigating the performance of MREs have also been developed [63][64][65][66].

MREs are generally fabricated from three thoroughly mixed primary components, including elastomeric material (matrix), magnetic filler particles, and additives [67]. The structure of MREs consists of micro- to nanosized filler magnetic particles, dispersed in a polymeric nonmagnetic matrix [68][69][70]. MREs have been fabricated from various types of matrix materials, such as natural rubber, polyurethane (PUR) rubber [71], silicone rubber (SR) [72], ethylene propylene diene rubber (EPDM) [73], and PDMS rubber [74]. Similarly, a variety of magnetic filler particles have been utilized in fabricating MREs, but bare iron particles (BIPs) [75] and carbonyl iron particles (CIPs) [76] are the most widely used magnetic filler particles. These particles are used in different shapes (sphere, flower, flake, and nugget) and sizes (5 to 100 μm). It has been reported that CIPs with an average diameter of 1–9 μm in the volume concentration from 25% to 30% offer ideal magnetic filler particle properties [31]. To further improve the properties of MREs, several additives, including plasticizers, silane coupling agents, and nanosized particles—such as carbon black, carbon nanotubes, graphite, and graphene—have also been incorporated [59][77]. Plasticizers improve elastomer mobility, matrix/filler affinity, and reduce the viscosity of matrix and storage modulus [78]. Silane coupling agents modify the surface properties of filler particles and improve their compatibility with the matrix [13]. Similarly, the addition of nanosized particles, particularly carbon black powder, increases the MR effects and tensile strength and decreases the damping ratio of MREs [24].

MREs can be classified into two groups based on the application of the magnetic field during vulcanization [79]. The MREs, cured without the application of the magnetic field and possessing uniformly distributed filler magnetic particles in the elastomeric matrix, are termed as isotropic MREs [80]. On the other hand, MREs cured in the presence of an external magnetic field and possessing a chainlike columnar structure with filler magnetic particles aligned along the applied magnetic field direction are known as anisotropic MREs [81]. Although the isotropic MREs provide smaller MR effects and relatively slow time response to the externally applied magnetic field than anisotropic MREs, their fabrication is much simpler and easier than anisotropic MREs. This is because the fabrication of anisotropic MREs needs a significantly high magnetic field strength (0.8 T) during crosslinking [24]. Additionally, upgraded rubber processing instruments and a properly designed setup to successfully apply the magnetic field are required to fabricate anisotropic MREs with improved properties. Furthermore, thicker anisotropic MREs cannot be fabricated, because an increase in the thickness of MRE rapidly decreases the magnetic flux density [24][82]. Isotropic MREs provide significant properties for a wide range of industrial applications at a low cost compared to anisotropic MREs. Due to these advantages, isotropic MREs are achieving great industrial importance nowadays [83]. Depending upon the applied magnetic field strength, the moduli of MREs immediately alter due to strong magnetic forces between magnetic filler particles. The ratio of change in moduli with an applied magnetic field to the initial modulus is called the MR effect [77][84]. Till now, different MR effects ranging from 4% to as high as 24,515% have been achieved [19]. Although the functionality, MR effect, and abrupt time response to the applied magnetic field of anisotropic MREs are much better than isotropic MREs, their fabrication is quite difficult compared to isotropic MREs [85].

2. Fabrication of Isotropic Magnetorheological Elastomers

MREs are composed of three major constituents: an elastomeric matrix, magnetic reinforcing particles, and additives. A variety of elastomeric materials, including liquid silicone [73], room temperature vulcanized (RTV)-based SR [31][45], high temperature vulcanized (HTV)-based SR [86], EPDM rubber [24], PUR [12][70], PDMS rubber [77][79], propylene rubber [30], SR resin [87], natural rubber (NR) [82], and scrub tire rubber [33] have been used for the fabrication of MREs. Among all, SR is the most extensively used rubber due to its unique properties such as room temperature vulcanization, ease of handling and processing, a wide range of operating temperatures, excellent hardness, stiffness [31], nontoxicity, and aging resistance [34]. Various magnetic reinforcing particles, i.e., BIPs [79][88], CIPs [21][69][89], Penta CIPs [90], magnetite (Fe_3O_4) [33], titanium dioxide (TiO_2) [61], and hard FeNdB [91] particles have been utilized for the fabrication of MREs. However, CIPs are the most commonly employed magnetic particles due to their high saturation magnetization and a wide range of particle size availability (1–200 μm) [91]. A fabricated MRE sample is illustrated in Figure 1, whereas various types of elastomeric matrices, magnetic filler particles, additives, and key parameters—used in the fabrication of isotropic MREs—are tabulated in Table 1.

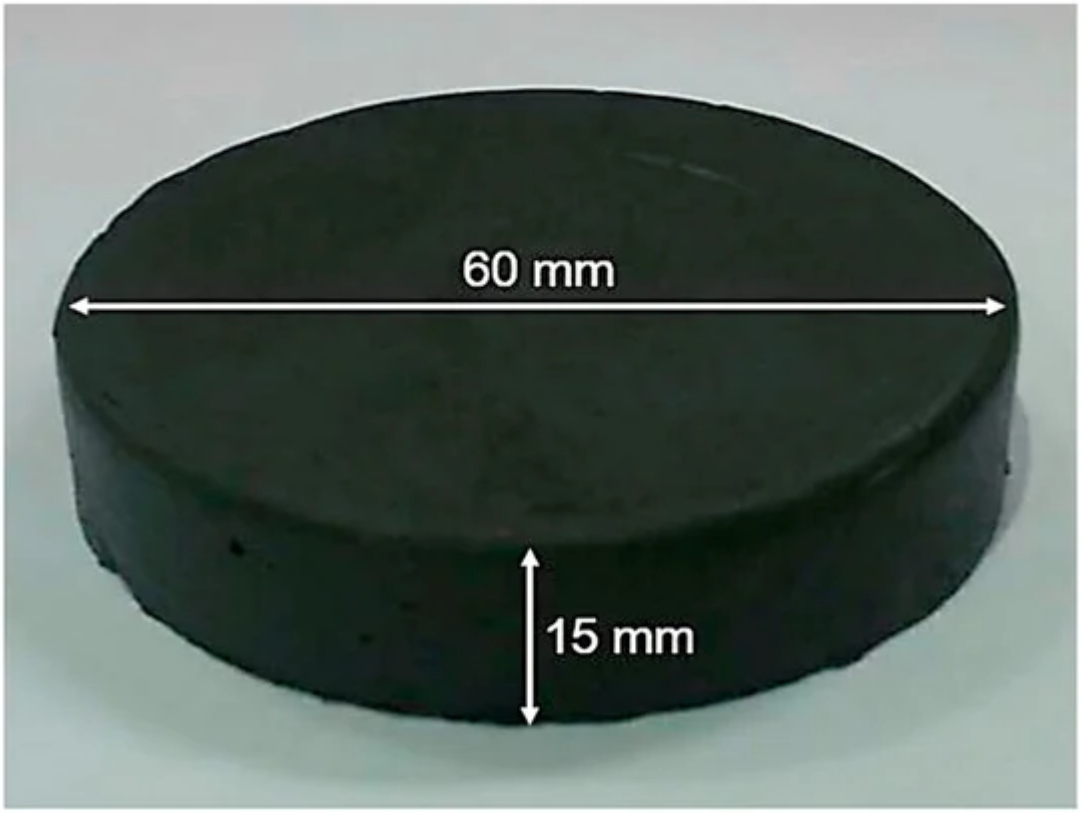

Figure 1. Fabricated isotropic magnetorheological elastomer (MRE) sample and its dimensions [34] (reprinted with permission from Elsevier™).

3. Fabrication of Isotropic Magnetorheological Elastomer

In the case of SR, the fabrication of isotropic MREs is quite easy and simple. The first step in SR-based MRE fabrication is the thorough mixing of liquid SR with suitable additives, such as catalyst [73], silicone oil (SO) [31], PDMS [45], graphene nanopowder [92], or 1,3-divinyl-1,1,3-tetramethyl disiloxane [22], and suitable magnetic filler

particles for sufficient time to obtain a uniform dispersion of particles in the solution [45]. The magnetic filler particles are usually added in the volume fractions, ranging from 5–40 vol%, whereas additives are added as per the required properties. Afterwards, this blend is placed inside a vacuum chamber for sufficient time to remove the trapped air bubbles during mixing [73]. After proper degassing, the blend is poured into plastic or metal molds. Then, the molds are again placed in the vacuum chamber for sufficient time for further degassing. As mentioned earlier, SR has the property of room temperature vulcanization, therefore, the solution is cured (vulcanized) in the molds at room temperature [23] or slightly higher temperature (65 °C) [93] after sufficient time, ranging from 10–2880 min [35] [45]. In the case of any other polymeric matrix, high-temperature vulcanization is carried out.

On the other hand, the PUR-based MREs are fabricated by mixing PUR rubber with additives (SO) and magnetic filler particles (CIPs) thoroughly at room temperature [12] or a slightly higher temperature (67 °C) [61]. This mixture is then poured into molds and cured at a specific temperature and pressure (20 KNm^{-2}) to get a final product [12][61]. Similarly, NR-based MREs are fabricated by mixing NR with filler particles homogeneously by two-roll mill or any other means and pouring into molds. Curing of NR-based MREs is performed in an oven, maintained at 180 °C under specific pressure (200 bar) for a specific time (10 min) to get the final isotropic MRE [27]. Furthermore, the fabrication of isotropic MRE from scrap tire rubber involves the separation of rubber from metals and fabrics, shredding into powder of 60-mesh size, and analyzing its chemical composition (usually 7% acetone extract, 5.45 ash, 32.9% carbon black, 54.6% hydrocarbon rubber). The Fe_3O_4 (60-mesh size) or Penta CIPs (6 µm) particles in 10–40 wt% are usually used as magnetic filler particles and sulfur, zinc oxide, stearic acid, and latex solutions as additives. The fabrication process of MREs from scrap tire rubber is comprised of several stages, including mixing of 100 phr of crumb rubber with 2 phr of sulfur, 1.5 phr of stearic acid, and 5 phr of zinc oxide for 15–30 min; addition of 15% latex solution; and further mixing for 15 min. Finally, the mixture is poured into molds and placed in a high-pressure high-temperature (HPHT) sintering device [92]. Sintering of molds was performed by applying a pressure of 25 MPa, heating to a temperature of 200 °C at a heating rate of 10 $°Cmin^{-1}$ within 17–20 min, and soaking at this temperature for 1 h. The hot molds are then cooled to room temperature. The volume fraction of produced MREs can be derived using Equation (1) [33].

$$\varphi = \frac{d_{MRE} - d_W}{d_{MP} - d_W}, \quad (1)$$

where d_{MRE} is the density of MREs, d_W is the density of pure reclaimed rubber, and d_{MP} is the density of magnetite powder. The base densities for the pure reclaimed rubber and magnetite powder were 1.107 gcm^{-3} and 5.27 gcm^{-3}, respectively [33][92].

4. Morphological Properties

Various characterization techniques—i.e., scanning electron microscopy (SEM), energy dispersive spectroscopy (EDS), X-ray photoelectron spectroscopy (XPS), Fourier transform infrared spectroscopy, and X-ray diffraction spectroscopy (XRD)—have been employed to explore the morphological properties of isotropic MREs. It has been

reported that the morphology of SR- and CIP-based MREs comprises homogeneously distributed CIPs throughout the SR matrix [34]. The large size CIPs of 6.25-µm diameter exhibit fairly uniform distribution, whereas small diameter CIPs produce agglomerates in the matrix. In the case of small diameter CIPs, the distance between particles was observed to be smaller and filler–filler particle interactions was greater, resulting in agglomeration of particles [94]. The addition of 10 wt% silicone oil causes more homogeneous dispersion of CIPs in the SR matrix without any structuring or surface defect [29]. SEM images, a histogram of particle size, XRD, FTIR spectra of SR, and CIP-based MREs, having PDMS as an additive, are illustrated in Figure 4. It was found that the morphology of CIPs-free MRE validated the formation of nonporous composite elastomers due to vulcanization under vacuum conditions (Figure 4a). On the other hand, Figure 4b demonstrated the random distribution of CIPs in the SR matrix. Similarly, Figure 4c,d confirmed the random distribution of CIPs with 2.5-mm average particle diameter in the SR matrix in the range of 0.5–4 mm. Two broad peaks at 12° and 23° in the XRD spectra validated the presence of PDMS and amorphous nature of SR-based polymer composite, whereas intense peaks at 44.8°, 65°, and 82.3° confirmed the presence and crystalline nature of CIPs (Figure 4e). The FTIR spectra of this MRE confirmed the asymmetric stretching vibration motion of Si–O–Si bond by absorption band at 800 cm^{-1} and the bending motion of Si–OH group by a peak near to 875 cm^{-1} (Figure 4f). The stretching vibrations of Si–O, and $Si(CH_3)_2$ groups were also validated by peaks in the range of 1000−1100 cm^{-1}. The additional absorption bands in the region of 1250 cm^{-1} and 2960 cm^{-1} presented the stretching vibration of $Si(CH_3)_2$ [23]. XPS spectra verified the results of FTIR spectroscopy, as illustrated in Figure 5.

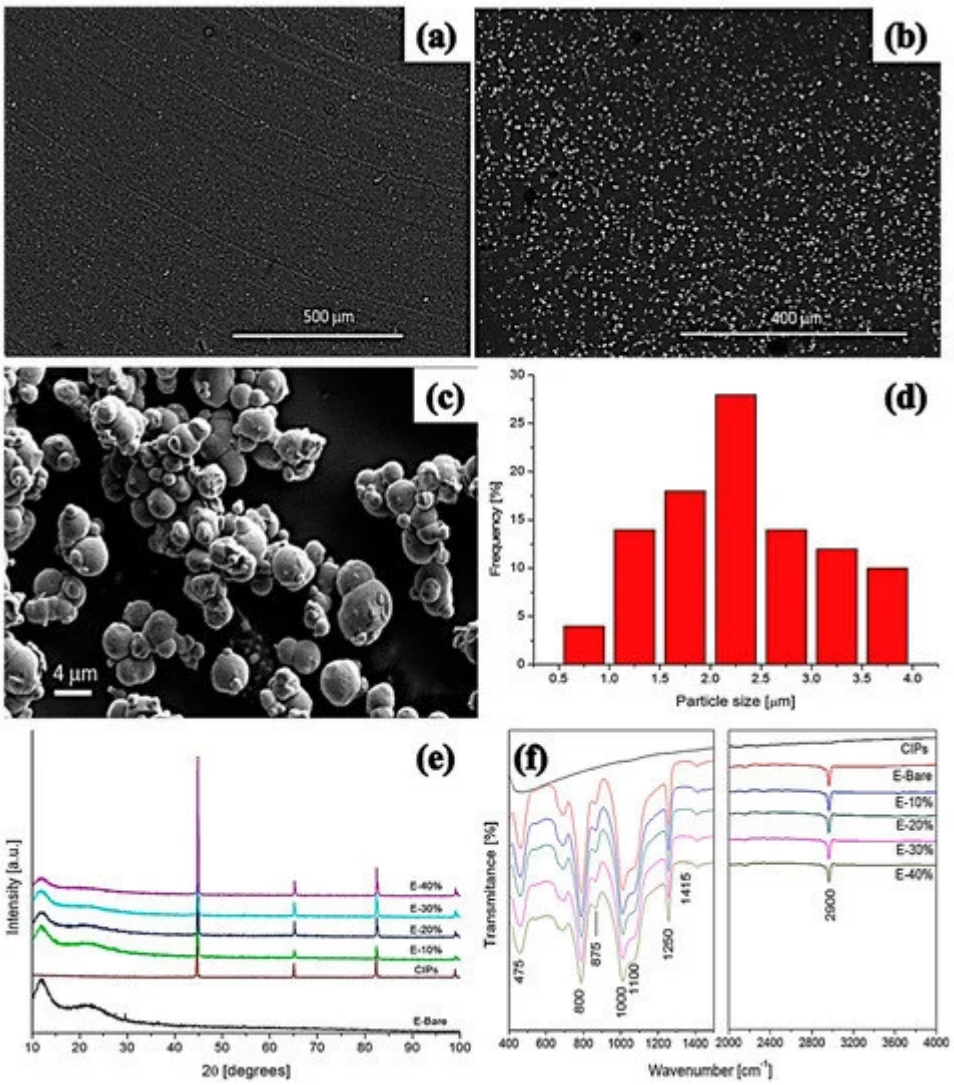

Figure 4. SEM micrographs of (**a**) CIPs-free MRE, (**b**) MRE with 20 wt% CIPs, (**c**) high-magnification micrograph of MRE, (**d**) histogram exhibiting CIPs size distribution in MREs, (**e**) XRD spectra, and (**f**) FTIR spectra of MREs [23] (reprinted with permission from Elsevier™).

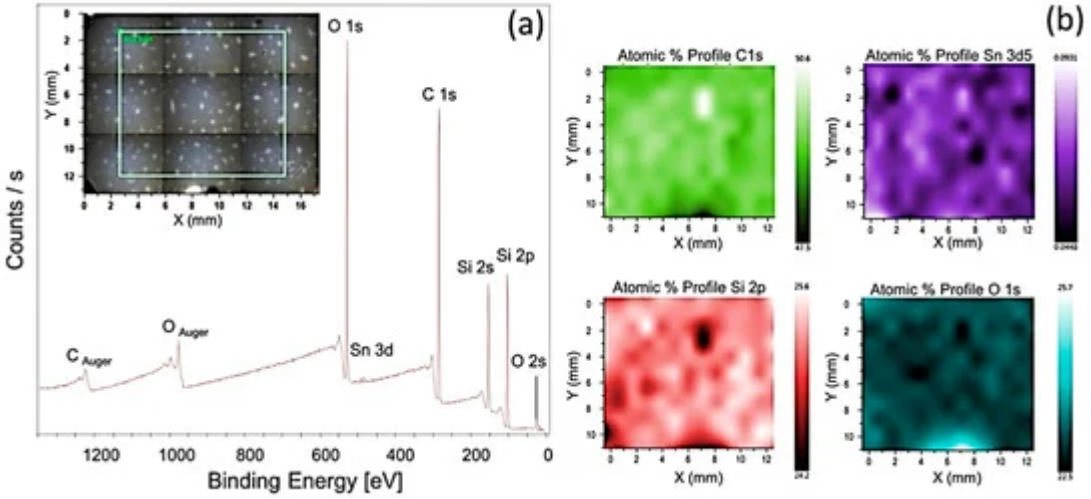

Figure 5. (**a**) XPS spectra of MRE with 20 wt% CIPs, demonstrating carbon, oxygen, silicon, and tin elements in the selected area, presented in inset figure. (**b**) XPS maps and atomic percentages of elements for the selected area [23] (reprinted with permission from Elsevier™).

It has also been reported that the CIPs of 4–5 μm diameter exhibit uniform distribution in EPDM- and CIP-based MRE, whereas CIPs of diameter 8−10 μm demonstrate aggregation of 2–3 particles. This aggregation begins with the addition of 10 phr of CIPs and 60 phr of carbon black in the EPDM. The MRE with 5 phr of CIPs demonstrated the fair distribution of single CIP within the EPDM matrix without aggregation. In two separate MREs, containing 30 phr of CIPs and 30 phr of BIPs of a diameter of 4–5 μm, a combination of single-particle distribution and aggregation of 2–3 particles was observed. But the MRE containing 30 phr of CIPs demonstrated a very homogeneous distribution compared to BIP-based MRE [24]. Cvek et al. [30] reported the uniform dispersion of CIPs in both virgin and reprocessed thermoplastic elastomer (TPE)-based matrix CIPs without agglomeration and air bubbles. On the other hand, the morphology of PUR-based MREs, containing pure CIPs and PANI-modified CIPs, have also been explored. Compared to pure CIP-based MREs, homogeneous and agglomerated free morphology was achieved in the PANI-modified CIP-based MREs. A particular self-assembled structure of modified CIPs and excellent compatibility between the CIPs and PUR was observed in the PANI-modified CIP-based MRE, attributed to the bridging of the CIPs/PUR covalent bonds [91].

5. Fatigue Life of MREs

The equi-biaxial fatigue life of SR- and CIP-based MREs were determined by the bubble inflation method. Figure 20 shows the plots of total energy density vs. cycles under various concentrations of CIPs. Variations in total energy density were observed to be highly sensitive to CIPs concentration and stress amplitude. For MREs with CIPs content ranging from 15% to 30%, a decrease in total energy density was observed with an increase in cycles at higher stress amplitudes, whereas an improvement in total energy density was achieved with an increase in cycles at lower stress amplitudes. Irrespective of the applied stress amplitude, total energy density improved with an increase in cycles in the case of MRE with 35% CIP content. A decrease in total energy density at failure was observed when drawn against log10 cycles. This fact suggested that the total energy could be used to predict the fatigue life of MREs subjected to equi-biaxial loading [35]. Uniaxial and biaxial cyclic fatigue properties of NR- and IP-based MREs were investigated between constant strain limits. The uniaxial cyclic fatigue test demonstrated that MREs exhibited stabilized properties at the latter stages of cyclic tests and any change in their properties was attributed to the applied magnetic flux density. An increase in the modulus from 1.325 MPa to 1.413 MPa was observed at the 360th cycle and at strain amplitudes ranging from 0.04–0.08. This was an approximate increase of 6.5% in the 50-cycle block average modulus attributed to the magnetic field applied at the 360th cycle. On the other hand, the block average modulus increased from 3.562 MPa to 3.591 MPa at the 350th cycle and at strain amplitudes ranging from 0.04–0.57. This was an approximate 0.8% increase in mean modulus of the 50-cycle block associated with the applied magnetic field at the 350th cycle. After comparison, it was concluded that increased strain amplitude decreases the MR effect attributed to the increase in separation distance between the particles and reduction in screening effects, whereas the biaxial bubble inflation cyclic fatigue test performed at a low strain of 0.0–0.1 and magnetic flux density of 198 mT showed that an increment in modulus from 3.066 MPa to

3.132 MPa was observed at the 90th cycle. This increment is attributed to the 2.2% improvement in block mean modulus under a specific magnetic flux density. Under the application of relatively higher strain (0–0.5) and the same magnetic flux density, an increment of 1% was observed at the 90th cycle in the block average modulus from 3.375 MPa to 3.410 MPa. In the case of strain amplitude ranging from 0.4–0.5 and the same magnetic flux density, an increment of 0.4% was observed in the MR effect at the 90th cycle from 3.553 MPa to 3.570 MPa [84].

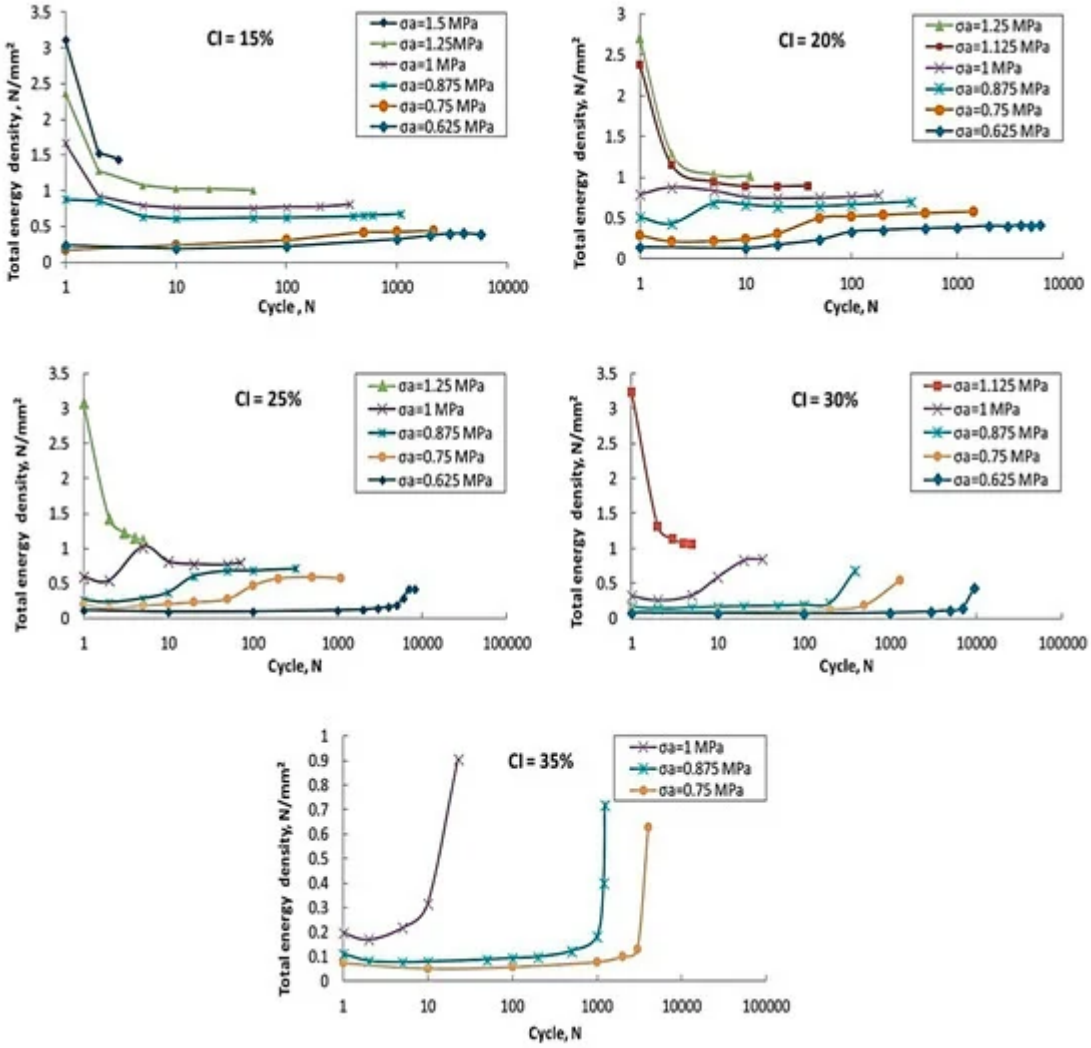

Figure 20. Plots of total energy density vs. cycles under different concentrations of CIPs [35] (reprinted with permission from Elsevier™).

References

1. Surbhi; Sukesha. Response of piezoelectric materials to the external temperature, electric field and humidity. Mater. Today Proc. 2020, 28, 1951–1954. [Google Scholar] [CrossRef]
2. Usman, M.; Hanif, A.; Kim, I.H.; Jung, H.J. Experimental validation of a novel piezoelectric energy harvesting system employing wake galloping phenomenon for a broad wind spectrum. Energy

2018, 153, 882–889. [Google Scholar] [CrossRef]

3. Bahmani, A.; Li, G.; Willett, T.L.; Montesano, J. Generating realistic representative microstructure of biomimetic composite materials for computational assessment of mechanical properties. Mater. Today Proc. 2019, 7, 373–381. [Google Scholar] [CrossRef]
4. Carotenuto, G.; La Peruta, G.; Nicolais, L. Thermo-chromic materials based on polymer-embedded silver clusters. Sensors Actuators B 2006, 114, 1092–1095. [Google Scholar] [CrossRef]
5. Yuan, X.; Zhou, X.; Liang, Y.; Wang, L.; Chen, R.; Zhang, M.; Pu, H.; Xuan, S.; Wu, J.; Wen, W. A stable high-performance isotropic electrorheological elastomer towards controllable and reversible circular motion. Compos. Part B 2020, 193, 107988. [Google Scholar] [CrossRef]
6. Usman, M.; Kim, I.H.; Jung, H.J. Improving thermoelectric energy harvesting efficiency by using graphene. AIP Adv. 2016, 6. [Google Scholar] [CrossRef]
7. Jiang, S.; Ichihashi, J.; Monobe, H.; Fujihira, M.; Ohtsu, M. Highly localized photochemical processes in LB films of photo chromic material by using a photon scanning tunneling microscope. Opt. Commun. 1994, 106, 173–177. [Google Scholar] [CrossRef]
8. Wang, B.; Kari, L. A visco-elastic-plastic constitutive model of isotropic magneto-sensitive rubber with amplitude, frequency and magnetic dependency. Int. J. Plast. 2020, 102756. [Google Scholar] [CrossRef]
9. Vaganov, M.V.; Borin, D.Y.; Odenbach, S.; Raikher, Y.L. Training effect in magnetoactive elastomers due to undermagnetization of magnetically hard filler. Phys. B Phys. Condens. Matter 2020, 578, 411866. [Google Scholar] [CrossRef]
10. Khayam, S.U.; Usman, M.; Umer, M.A.; Rafique, A. Development and characterization of a novel hybrid magnetorheological elastomer incorporating micro and nano size iron fillers. Mater. Des. 2020, 192. [Google Scholar] [CrossRef]
11. Velmurugan, C.; Senthilkumar, V.; Kesavan, J.; Ramya, K. Effects of sintering temperature on grain growth of NiTiCu shape memory alloy. Mater. Today Proc. 2020. [Google Scholar] [CrossRef]
12. Bica, I.; Anitas, E.M.; Marina, L.; Averis, E.; Hyuk, S.; Jin, H. Magnetostrictive and viscoelastic characteristics of polyurethane-based magnetorheological elastomer. J. Ind. Eng. Chem. 2019, 73, 128–133. [Google Scholar] [CrossRef]
13. Li, Y.; Li, J.; Li, W.; Du, H. A state-of-the-art review on magnetorheological elastomer devices. Smart Mater. Struct. 2014, 23, 123001. [Google Scholar] [CrossRef]
14. Fu, J.; Bai, J.; Lai, J.; Li, P.; Yu, M.; Lam, H. Adaptive fuzzy control of a magnetorheological elastomer vibration isolation system with time-varying sinusoidal excitations. J. Sound Vib. 2019,

456, 386–406. [Google Scholar] [CrossRef]

15. Akhavan, H.; Ghadiri, M.; Zajkani, A. A new model for the cantilever MEMS actuator in magnetorheological elastomer cored sandwich form considering the fringing field and Casimir effects. Mech. Syst. Signal Process. 2019, 121, 551–561. [Google Scholar] [CrossRef]
16. Eshaghi, M. The effect of magnetorheological fluid and aerodynamic damping on the flutter boundaries of MR fluid sandwich plates in supersonic airflow. Eur. J. Mech./A Solids 2020, 82, 103997. [Google Scholar] [CrossRef]
17. Kumar, J.S.; Alex, D.G.; Paul, P.S. Synthesis of Magnetorheological fluid Compositions for Valve Mode Operation. Mater. Today Proc. 2020, 22, 1870–1877. [Google Scholar] [CrossRef]
18. Wang, N.; Liu, X.; Sun, S.; Królczyk, G.; Li, Z.; Li, W. Microscopic characteristics of magnetorheological fl uids subjected to magnetic fi elds. J. Magn. Magn. Mater. 2020, 501, 166443. [Google Scholar] [CrossRef]
19. Vatandoost, H.; Hemmatian, M.; Sedaghati, R.; Rakheja, S. Dynamic characterization of isotropic and anisotropic magnetorheological elastomers in the oscillatory squeeze mode superimposed on large static pre-strain. Compos. Part B Eng. 2020, 182, 107648. [Google Scholar] [CrossRef]
20. Wen, Q.; Shen, L.; Li, J.; Xuan, S.; Li, Z.; Fan, X.; Li, B. Temperature dependent magneto-mechanical properties of magnetorheological elastomers. J. Magn. Magn. Mater. 2020, 497, 165998. [Google Scholar] [CrossRef]
21. Hegde, S.; Poojary, U.R.; Gangadharan, K.V. Experimental investigation of effect of ingredient particle size on dynamic damping of RTV silicon base magnetorheological elastomer. Procedia Mater. Sci. 2014, 5, 2301–2309. [Google Scholar] [CrossRef]
22. Schümann, M.; Odenbach, S. In-situ observation of the particle microstructure of magnetorheological elastomers in presence of mechanical strain and magnetic fields. J. Magn. Magn. Mater. 2017, 441, 88–92. [Google Scholar] [CrossRef]
23. Perales-Martínez, I.A.; Palacios-Pineda, L.M.; Lozano-Sánchez, L.M.; Martínez-Romero, O.; Puente-Cordova, J.G.; Elías-Zúñiga, A. Enhancement of a magnetorheological PDMS elastomer with carbonyl iron particles. Polym. Test. 2017, 57, 78–86. [Google Scholar] [CrossRef]
24. Burgaz, E.; Goksuzoglu, M. Effects of magnetic particles and carbon black on structure and properties of magnetorheological elastomers. Polym. Test. 2020, 81, 106233. [Google Scholar] [CrossRef]
25. Chikh, N. Dynamic Analysis of the Non-Linear Behavior of a Composite Sandwich Beam with a Magnetorheological. Acta Mech. Solida Sin. 2016, 29, 271–283. [Google Scholar] [CrossRef]
26. Usman, M.; Jang, D.-D.; Kim, I.; Jung, H.-J.; Koo, J. Dynamic testing and modeling of magneto-rheological elastomers. In Proceedings of the ASME 2009 Conference on Smart Materials,

Adaptive Structures and Intelligent Systems, Oxnard, CA, USA, 21–23 September 2009; ASME: New York, NY, USA, 2009; Volume 48968, pp. 495–500. [Google Scholar]

27. Agirre-Olabide, I.; Elejabarrieta, M.J. A new magneto-dynamic compression technique for magnetorheological elastomers at high frequencies. Polym. Test. 2018, 66, 114–121. [Google Scholar] [CrossRef]
28. Kumbhar, S.B.; Chavan, S.P.; Gawade, S.S. Two Way Stiffness Tuning Of Magnetorheological Elastomer- Shape Memory Alloy Composite. Mater. Today Proc. 2018, 5, 13211–13219. [Google Scholar] [CrossRef]
29. Gao, W.; Wang, X. Experimental and theoretical investigations on magnetoelastic shear behavior of isotropic MR elastomers under gradient magnetic fi elds. J. Magn. Magn. Mater. 2019, 483, 196–204. [Google Scholar] [CrossRef]
30. Cvek, M.; Kracalik, M.; Sedlacik, M.; Mrlik, M.; Sedlarik, V. Reprocessing of injection-molded magnetorheological elastomers based on TPE matrix. Compos. Part B 2019, 172, 253–261. [Google Scholar] [CrossRef]
31. Shenoy, K.P.; Poojary, U.; Gangadharan, K.V. A novel approach to characterize the magnetic field and frequency dependent dynamic properties of magnetorheological elastomer for torsional loading conditions. J. Magn. Magn. Mater. 2020, 498, 166169. [Google Scholar] [CrossRef]
32. Mazlan, S.A.; Sutrisno, J.; Yahya, I.; Imaduddin, F. Physicochemical properties and stress-strain compression behaviors of a ground tire rubber based magnetorheological elastomers. Sci. Iran. Trans. C Chem. Chem. Eng. 2016, 23, 1144–1159. [Google Scholar]
33. Imaduddin, F.; Li, Y.; Mazlan, S.A.; Sutrisno, J.; Koga, T.; Yahya, I.; Choi, S.B. A new class of magnetorheological elastomers based on waste tire rubber and the characterization of their properties. Smart Mater. Struct. 2016, 25, 115002. [Google Scholar]
34. Lian, C.; Lee, K.; Lee, C. Friction and wear characteristics of magnetorheological elastomer under vibration conditions. Tribiology Int. 2016, 98, 292–298. [Google Scholar] [CrossRef]
35. Zhou, Y.; Jiang, L.; Chen, S.; Ma, J.; Betts, A.; Jerrams, S. Determination of reliable fatigue life predictors for magnetorheological elastomers under dynamic equi-biaxial loading. Polym. Test. 2017, 61, 177–184. [Google Scholar] [CrossRef]
36. Shu, Q.; Ding, L.; Gong, X.; Hu, T.; Xuan, S. High performance magnetorheological elastomers strengthened by perpendicularly interacted flax fiber and carbonyl iron chains. Smart Mater. Struct. 2020, 29, 25010. [Google Scholar] [CrossRef]
37. Bao, X.; Komatsuzaki, T.; Zhang, N. A nonlinear magnetorheological elastomer model based on fractional viscoelasticity, magnetic dipole interactions, and adaptive smooth Coulomb friction. Mech. Syst. Signal Process. 2019, 141, 106438. [Google Scholar]

38. Xu, Z.; Tong, J.; Wu, F. Magnetorheological elastomer vibration isolation of tunable three-dimensional locally resonant acoustic metamaterial. Solid State Commun. 2018, 271, 51–55. [Google Scholar] [CrossRef]
39. Komatsuzaki, T.; Inoue, T.; Terashima, O. Broadband vibration control of a structure by using a magnetorheological elastomer-base d tuned dynamic absorber. Mechatronics 2016, 40, 128–136. [Google Scholar] [CrossRef]
40. Ausanio, G.; Iannotti, V.; Ricciardi, E.; Lanotte, L.; Lanotte, L. Magneto-piezoresistance in Magnetorheological elastomers for magnetic induction gradient or position sensors. Sensors Actuators A Phys. 2014, 205, 235–239. [Google Scholar] [CrossRef]
41. Bajkowski, J.M.; Bajer, I. Semi-active control of a sandwich beam partially filled with magnetorheological elastomer. Mech. Syst. Signal Process. 2015, 61, 695–705. [Google Scholar]
42. Ladipo, I.L.; Fadly, J.D.; Faris, W.F. Characterization of Magnetorheological Elastomer (MRE) Engine mounts. Mater. Today Proc. 2016, 3, 411–418. [Google Scholar] [CrossRef]
43. Xu, Z.; Wu, H.; Wang, Q.; Jiang, S.; Yi, L.; Wang, J. Study on movement mechanism of magnetic particles in silicone rubber- based magnetorheological elastomers with viscosity change. J. Magn. Magn. Mater. 2020, 494, 165793. [Google Scholar] [CrossRef]
44. Gu, X.; Li, J.; Li, Y. Experimental realisation of the real-time controlled smart magnetorheological elastomer seismic isolation system with shake table. Struct. Control Heal. Monit. 2020, 27, 1–24. [Google Scholar] [CrossRef]
45. Yu, Y.; Li, Y.; Li, J.; Gu, X. Self-adaptive step fruit fly algorithm optimized support vector regression model for dynamic response prediction of magnetorheological elastomer base isolator. Neurocomputing 2016, 211, 41–52. [Google Scholar] [CrossRef]
46. Gu, X.; Yu, Y.; Li, Y.; Li, J.; Askari, M.; Samali, B. Experimental study of semi-active magnetorheological elastomer base isolation system using optimal neuro fuzzy logic control. Mech. Syst. Signal Process. 2019, 119, 380–398. [Google Scholar] [CrossRef]
47. Bao, X.; Komatsuzaki, T.; Iwata, Y.; Asanuma, H. Modeling and semi-active fuzzy control of magnetorheological elastomer-based isolator for seismic response reduction. Mech. Syst. Signal Process. 2018, 101, 449–466. [Google Scholar]
48. Tao, Y.; Rui, X.; Yang, F.; Hao, B. Development of a MRE isolation system for strapdown inertial measurement unit. Mech. Syst. Signal Process. 2019, 117, 553–568. [Google Scholar] [CrossRef]
49. Yang, J.; Sun, S.; Tian, T.; Li, W.; Du, H. Development of a novel multi-layer MRE isolator for suppression of building vibrations under seismic events. Mech. Syst. Signal Process. 2016, 70–71, 811–820. [Google Scholar] [CrossRef]

50. Barman, H.; Hegde, S. Comprehensive review of parameters influencing the performance of magnetorheological elastomers embedded in beams. Mater. Today Proc. 2020, 26, 2130–2135. [Google Scholar] [CrossRef]
51. Tong, Y.; Dong, X.; Qi, M. Payne effect and damping properties of flower-like cobalt particles-based magnetorheological elastomers. Compos. Commun. 2019, 15, 120–128. [Google Scholar] [CrossRef]
52. Praveen, T.; Dwivedy, S.K. Dynamic analysis of MRE embedded sandwich plate using FEM. Procedia Eng. 2016, 144, 721–728. [Google Scholar]
53. Bornassi, S.; Navazi, H.M.; Haddadpour, H. Thin-Walled Structures Aeroelastic instability analysis of a turbomachinery cascade with magnetorheological elastomer based adaptive blades. Thin Walled Struct. 2018, 130, 71–84. [Google Scholar] [CrossRef]
54. Mikhailov, V.P.; Bazinenkov, A.M. Active vibration isolation platform on base of magnetorheological elastomers. J. Magn. Magn. Mater. 2017, 431, 266–268. [Google Scholar] [CrossRef]
55. Usman, M.; Sung, S.H.; Jang, D.D.; Jung, H.J.; Koo, J.H. Numerical investigation of smart base isolation system employing MR elastomer. J. Phys. Conf. Ser. 2009, 149, 012099. [Google Scholar] [CrossRef]
56. Koo, J.H.; Jang, D.D.; Usman, M.; Jung, H.J. A feasibility study on smart base isolation systems using magneto-rheological elastomers. Struct. Eng. Mech. 2009, 32, 755–770. [Google Scholar] [CrossRef]
57. Bocian, M.; Kaleta, J.; Lewandowski, D.; Przybylski, M. Tunable Absorption System based on magnetorheological elastomers and Halbach array: Design and testing. J. Magn. Magn. Mater. 2017, 435, 46–57. [Google Scholar] [CrossRef]
58. Sun, S.S.; Yang, J.; Li, W.H.; Du, H.; Alici, G.; Yan, T.H.; Nakano, M. Development of an isolator working with magnetorheological elastomers and fluids. Mech. Syst. Signal Process. 2017, 83, 371–384. [Google Scholar] [CrossRef]
59. Balasoiu, M.; Bica, I. Composite magnetorheological elastomers as dielectrics for plane capacitors: Effects of magnetic field intensity. Results Phys. 2016, 6, 199–202. [Google Scholar] [CrossRef]
60. Babu, R.; Rajamohan, V.; Sudhagar, P.E. Structural optimization of tapered composite sandwich plates partially treated with magnetorheological elastomers. Compos. Struct. 2018, 200, 258–276. [Google Scholar]
61. Yuan, L.; Sun, S.; Pan, Z.; Ding, D.; Gienke, O.; Li, W. Mode coupling chatter suppression for robotic machining using semi-active magnetorheological elastomers absorber. Mech. Syst. Signal Process. 2019, 117, 221–237. [Google Scholar] [CrossRef]

62. Hooshiar, A.; Alkhalaf, A.; Dargahi, J. Development and assessment of a stiffness display system for minimally invasive surgery based on smart magneto-rheological elastomers. Mater. Sci. Eng. C 2020, 108, 110409. [Google Scholar] [CrossRef] [PubMed]
63. Keip, M.; Rambausek, M. Computational and analytical investigations of shape effects in the experimental characterization of magnetorheological elastomers. Int. J. Solids Struct. 2017, 121, 1–20. [Google Scholar] [CrossRef]
64. Gu, X.; Yu, Y.; Li, J.; Li, Y. Semi-active control of magnetorheological elastomer base isolation system utilising learning-based inverse model. J. Sound Vib. 2017, 406, 346–362. [Google Scholar] [CrossRef]
65. Mukherjee, D.; Bodelot, L.; Danas, K. Microstructurally-guided explicit continuum models for isotropic magnetorheological elastomers with iron particles. Int. J. Non. Linear. Mech. 2020, 120, 103380. [Google Scholar] [CrossRef]
66. Usman, M.; Ahmed, S.; Jung, H.-J. State-Switched Control Algorithm fo Multi Degree of Freedom Smart Base Isolation System Employing MR Elastomer. In Proceedings of the International Conference on Earthquake Engineering ans Seismology, Islamabad, Pakistan, 25–26 April 2011. [Google Scholar]
67. Yu, M.; Ju, B.; Fu, J.; Liu, X.; Yang, Q. Influence of composition of carbonyl iron particles on dynamic mechanical properties of magnetorheological elastomers. J. Magn. Magn. Mater. 2012, 324, 2147–2152. [Google Scholar] [CrossRef]
68. Boczkowska, A.; Awietjan, S.F.; Pietrzko, S.; Kurzydłowski, K.J. Mechanical properties of magnetorheological elastomers under shear deformation. Compos. Part B 2012, 43, 636–640. [Google Scholar] [CrossRef]
69. de Souza Eloy, F.; Gomes, G.F.; Ancelotti, A.C., Jr.; da Cunha, S.S., Jr.; Bombard, A.J.; Junqueira, D.M. A numerical-experimental dynamic analysis of composite sandwich beam with magnetorheological elastomer honeycomb core. Compos. Struct. 2019, 209, 242–257. [Google Scholar] [CrossRef]
70. Bao, X.; Komatsuzaki, T.; Iwata, Y. Robust adaptive controller for semi-active control of uncertain structures using a magnetorheological elastomer-based isolator. J. Sound Vib. 2018, 434, 192–212. [Google Scholar]
71. Marvalov, B. Experimental characterization and viscoelastic modeling of isotropic and anisotropic magnetorheological elastomers. Polym. Test. 2020, 81, 106272. [Google Scholar]
72. Bica, I. The influence of the magnetic field on the elastic properties of anisotropic magnetorheological elastomers. J. Ind. Eng. Chem. 2012, 18, 1666–1669. [Google Scholar] [CrossRef]

73. Khimi, S.R.; Pickering, K.L. The effect of silane coupling agent on the dynamic mechanical properties of iron sand/natural rubber magnetorheological elastomers. Compos. Part B 2016, 90, 115–125. [Google Scholar] [CrossRef]
74. Ge, L.; Gong, X.; Wang, Y.; Xuan, S. The conductive three dimensional topological structure enhanced magnetorheological elastomer towards a strain sensor. Compos. Sci. Technol. 2016, 135, 92–99. [Google Scholar] [CrossRef]
75. Winger, J.; Schümann, M.; Kupka, A.; Odenbach, S. Influence of the particle size on the magnetorheological effect of magnetorheological elastomers. J. Magn. Magn. Mater. 2019, 481, 176–182. [Google Scholar] [CrossRef]
76. Hapipi, N.; Aishah, S.; Aziz, A.; Amri, S.; Bok, S.; Mohamad, N.; Hana, M.; Khairi, A.; Yasser, A.; Fatah, A.; et al. The field-dependent rheological properties of plate-like carbonyl iron particle-based magnetorheological elastomers. Results Phys. 2019, 12, 2146–2154. [Google Scholar] [CrossRef]
77. Bunoiu, M.; Bica, I. Magnetorheological elastomer based on silicone rubber, carbonyl iron and Rochelle salt: Effects of alternating electric and static magnetic fields intensities. J. Ind. Eng. Chem. 2016, 37, 312–318. [Google Scholar] [CrossRef]
78. Bocian, M.; Kaleta, J.; Lewandowski, D.; Przybylski, M. Test setup for examination of magneto-mechanical properties of magnetorheological elastomers with use of a novel approach. Arch. Civ. Mech. Eng. 2016, 16, 294–303. [Google Scholar] [CrossRef]
79. Khanouki, M.A.; Sedaghati, R.; Hemmatian, M. Experimental characterization and microscale modeling of isotropic and anisotropic magnetorheological elastomers. Compos. Part B 2019, 176, 107311. [Google Scholar] [CrossRef]
80. Gorman, D.; Murphy, N.; Ekins, R.; Jerrams, S. The evaluation of the effect of strain limits on the physical properties of Magnetorheological Elastomers subjected to uniaxial and biaxial cyclic testing. Int. J. Fatigue 2017, 103, 1–4. [Google Scholar] [CrossRef]
81. Masbowski, M.; Miedzianowska, J.; Strzelec, K. Reinforced, extruded, isotropic magnetic elastomer composites: Fabrication and properties. Adv. Polym. Technol. 2019, 2019, 3517430. [Google Scholar]
82. Alkhalaf, A.; Hooshiar, A.; Dargahi, J. Composite magnetorheological elastomers for tactile displays: Enhanced MR-effect through bi-layer composition. Compos. Part B 2020, 190, 107888. [Google Scholar] [CrossRef]
83. Rudykh, S.; Bertoldi, K. Stability of anisotropic magnetorheological elastomers in finite deformations: A micromechanical approach. J. Mech. Phys. Solids 2013, 61, 949–967. [Google Scholar] [CrossRef]

84. Liao, G.; Gong, X.; Xuan, S. In fluence of shear deformation on the normal force of magnetorheological elastomer. Mater. Lett. 2013, 106, 270–272. [Google Scholar] [CrossRef]
85. Bastola, A.K.; Li, L. A new type of vibration isolator based on magnetorheological elastomer. Mater. Des. 2018, 157, 431–436. [Google Scholar] [CrossRef]
86. Gorman, D.; Murphy, N.; Ekins, R.; Jerrams, S. The evaluation and implementation of magnetic fields for large strain uniaxial and biaxial cyclic testing of Magnetorheological Elastomers. Polym. Test. 2016, 51, 74–81. [Google Scholar] [CrossRef]
87. Yu, M.; Qi, S.; Fu, J.; Zhu, M.; Chen, D. Understanding the reinforcing behaviors of polyaniline-modified carbonyl iron particles in magnetorheological elastomer based on polyurethane/epoxy resin IPNs matrix. Compos. Sci. Technol. 2017, 139, 36–46. [Google Scholar] [CrossRef]
88. Choi, H.J.; Mazlan, S.A.; Imaduddin, F. Fabrication and viscoelastic characteristics of waste tire rubber based magnetorheological elastomer. Smart Mater. Struct. 2016, 25, 115026. [Google Scholar]
89. Stepanov, G.V.; Chertovich, A.V.; Kramarenko, E.Y. Magnetorheological and deformation properties of magnetically controlled elastomers with hard magnetic filler. J. Magn. Magn. Mater. 2012, 324, 3448–3451. [Google Scholar] [CrossRef]
90. Qian, D.Y.; Hussain, M.; Zheng, Z.G.; Zhong, X.C.; Gao, X.X.; Liu, Z.W. Compositional optimization for nanocrystalline hard magnetic MRE–Fe–B–Zr alloys via modifying RE and B contents. J. Magn. Magn. Mater. 2015, 384, 87–92. [Google Scholar] [CrossRef]
91. Dargahi, A.; Sedaghati, R.; Rakheja, S. On the properties of magnetorheological elastomers in shear mode: Design, fabrication and characterization. Compos. Part B Eng. 2019, 159, 269–283. [Google Scholar] [CrossRef]
92. Bica, I.; Anitas, E.M.; Chirigiu, L. Magnetic field intensity effect on plane capacitors based on hybrid magnetorheological elastomers with graphene nanoparticles. J. Ind. Eng. Chem. 2017, 56, 407–412. [Google Scholar] [CrossRef]
93. Dargahi, A.; Sedaghati, R.; Rakheja, S. On the properties of magnetorheological elastomers in shear mode: Design, fabrication and characterization. Compos. Part B Eng. 2019, 159, 269–283. [Google Scholar] [CrossRef]
94. Moksin, N.; Ismail, H.; Abdullah, M.K.; Shuib, R.K. Magnetorheological elastomer composites based on industrial waste nickel zinc ferrite and natural rubber. Rubber Chem. Technol. 2019, 92, 749–762. [Google Scholar] [CrossRef]
95. Dargahi, A.; Sedaghati, R.; Rakheja, S. On the properties of magnetorheological elastomers in shear mode: Design, fabrication and characterization. Compos. Part B Eng. 2019, 159, 269–283. [Google Scholar] [CrossRef]

96. Bica, I.; Anitas, E.M.; Chirigiu, L. Magnetic field intensity effect on plane capacitors based on hybrid magnetorheological elastomers with graphene nanoparticles. J. Ind. Eng. Chem. 2017, 56, 407–412. [Google Scholar] [CrossRef]

97. Moksin, N.; Ismail, H.; Abdullah, M.K.; Shuib, R.K. Magnetorheological elastomer composites based on industrial waste nickel zinc ferrite and natural rubber. Rubber Chem. Technol. 2019, 92, 749–762. [Google Scholar] [CrossRef]